

The following resources related to this article are available online at www.sciencemag.org (this information is current as of January 1, 2010):

Updated information and services, including high-resolution figures, can be found in the online version of this article at:

<http://www.sciencemag.org/cgi/content/full/303/5654/65>

Supporting Online Material can be found at:

<http://www.sciencemag.org/cgi/content/full/303/5654/65/DC1>

This article **cites 15 articles**, 10 of which can be accessed for free:

<http://www.sciencemag.org/cgi/content/full/303/5654/65#otherarticles>

This article has been **cited by** 130 article(s) on the ISI Web of Science.

This article appears in the following **subject collections**:

Chemistry

<http://www.sciencemag.org/cgi/collection/chemistry>

Information about obtaining **reprints** of this article or about obtaining **permission to reproduce this article** in whole or in part can be found at:

<http://www.sciencemag.org/about/permissions.dtl>

proach of functionalizing the entrance to each CNT core can be generalized to a variety of biological affinity pairs to block ionic flow through the CNT core when the analyte is present.

Electrochemistry can also be used to tailor the aligned CNT membrane structure. Practical considerations of membrane strength and aligned CNT growth require that the membrane be at least 5 μm thick. However, for large molecular separations based on gate-keeper selectivity, a short path length is desired, because it increases the diffusion flux. One possible route to trim the CNT length is to anodically oxidize the CNTs at +1.7 V versus an Ag-AgCl reference electrode (26). Because the PS polymer is an insulator, the conductive CNTs are selectively etched within the polymer matrix. Thus, one can adjust pore length while maintaining the mechanical integrity of the thicker PS matrix. Figure 4A shows the surface of membrane films after H_2O plasma oxidation. The tips of the CNTs are extending above the surface because of the faster etching rate of PS by plasma treatment. Each bright area in Fig. 4A corresponds to the tips of multiple (2–7) CNTs clustered together, resulting in outer diameters of ~ 50 nm that are consistent with TEM observations. An areal density of $6 (\pm 3) \times 10^{10}$ per cm^2 can be estimated from this micrograph. Figure 4B shows a schematic cross section illustration of how CNTs could be selectively oxidized electrochemically inside an insulating PS matrix. Figure 4C shows the surface after selective electrochemical oxidation. The size of the pores on the PS surface should be at least that of the 40-nm outer CNT diameter (Fig. 4B). Because the tips of the CNTs tend to group together and there is the possibility of localized PS oxidation next to the CNTs, the resulting PS surface pores were often greater than 100 nm. Figure 4C (arrow) shows an example of a smaller PS surface pore inside a larger PS surface pore, which is consistent with clustering of CNT tips at the surface.

Selective reduction of the length of CNTs within the PS matrix can be a valuable tool for tuning membranes to give a required flux while keeping carboxylate functionalization at the tips of CNTs. These carboxylate end groups can then be readily functionalized at the entrance of each CNT inner core to selectively gate molecular transport through the ordered nanoporous membrane for separation and sensing applications.

References and Notes

1. E. Klein, *J. Membr. Sci.* **179**, 1 (2000).
2. T. Thurn-Albrecht et al., *Adv. Mater.* **12**, 787 (2000).
3. J. T. Asefa, M. J. MacLachlan, N. Coombs, G. A. Ozin, *Nature* **402**, 867 (1999).
4. K. B. Jirage, J. C. Hulthen, C. R. Martin, *Science* **278**, 655 (1997).
5. E. D. Steinle et al., *Anal. Chem.* **74**, 2416 (2002).
6. S. B. Lee et al., *Science* **296**, 2198 (2002).
7. H. Kanzow, C. Lenski, A. Ding, *Phys. Rev. B* **63**, 12, 5402 (2001).

8. H. Ago, T. Komatsu, S. Ohshima, Y. Kuriki, M. Yumura, *Appl. Phys. Lett.* **77**, 79 (2000).
9. L. Sun, R. M. Crooks, *J. Am. Chem. Soc.* **122**, 12340 (2000).
10. S. A. Miller, C. R. Martin, *J. Electroanal. Chem.* **522**, 66 (2002).
11. H. Ago, T. Komatsu, S. Ohshima, Y. Kuriki, M. Yumura, *Appl. Phys. Lett.* **77**, 79 (2000).
12. C. L. Cheung, A. Kurtz, H. Park, C. Lieber, *J. Phys. Chem. B* **106**, 2429 (2002).
13. M. J. Casavant, D. A. Walters, J. J. Schmidt, R. E. Smalley, *J. Appl. Phys.* **93**, 2153 (2003).
14. R. Andrews et al., *Chem. Phys. Lett.* **303**, 467 (1999).
15. Z. F. Ren et al., *Science* **282**, 1105 (1998).
16. V. I. Merkulov et al., *Appl. Phys. Lett.* **80**, 4816 (2002).
17. Z. J. Zhang, B. Q. Wei, G. Ramanath, P. M. Ajayan, *Appl. Phys. Lett.* **77**, 3764 (2000).
18. Materials and methods are available as supporting material on Science Online.
19. D. Qian, E. C. Dickey, R. Andrews, T. Rantell, *Appl. Phys. Lett.* **76**, 2868 (2000).
20. S. M. Huang, L. M. Dai, *J. Phys. Chem. B* **106**, 3543 (2002).
21. M. A. Hamon, H. Hui, P. Bhowmik, H. M. E. Itkis, R. C. Haddon, *Appl. Phys. A* **74**, 333 (2002).
22. C. V. Nguyen et al., *Nano Letters* **2**, 1079 (2002).

23. J. L. Bahr, J. M. Tour, *Chem. Mater.* **13**, 3823 (2001).
24. X. Pages, V. Rouessac, D. Cot, G. Nabias, J. Durand, *Sep. Purif. Tech.* **25**, 399 (2001).
25. D. O. Wipf, E. W. Kristensen, M. R. Deakin, R. M. Wightman, *Anal. Chem.* **60**, 306 (1988).
26. T. Ito, L. Sun, R. M. Crooks, *Electrochem. Solid State Lett.* **6**, C4 (2003).
27. We thank W. Shafer for porosity measurements, D. Qian for the growth of aligned CNTs, A. Jeromczyk for aid with electrochemical measurements, and A. Dozier for aid with TEM characterization. Supported by a Kentucky Science and Engineering Foundation seed grant, by the NSF Materials Research Science and Engineering Center's Advanced Carbon Materials Center (grant no. DMR-9809686), and by NASA and Air Force Research Laboratory (agreement no. F49620-02-1-0225).

Supporting Online Material

www.sciencemag.org/cgi/content/full/1092048/DC1
Materials and Methods
Figs. S1 to S3

9 September 2003; accepted 17 November 2003
Published online 27 November 2003;
10.1126/science.1092048
Include this information when citing this paper.

Supramolecular Self-Assembly of Macroscopic Tubes

Deyue Yan,* Yongfeng Zhou, Jian Hou

The macroscopic molecular self-assembly of an amphiphilic hyperbranched copolymer in acetone generated multiwalled tubes millimeters in diameter and centimeters in length. The thickness of the tube walls approaches 400 nanometers, and the walls have an inhomogeneous lamella structure that alternates between ordered hydrophilic domains and amorphous, partly irregular hydrophilic domains.

Molecular self-assembly of organic molecules has generated a wide variety of objects with nanoscale or micrometer-scale morphologies, including micelles (1, 2), vesicles (3–5), ribbons (6), films (7), fibers (8–10), and tubules (11–13). These reported self-assembled objects were predominantly generated from organic molecules with well-defined size and structure. To date, little attention has been paid to molecular self-assembly originating from ill-defined macromolecules such as hyperbranched copolymers. We now report the molecular self-assembly of tubes with macroscopic dimensions.

When an amphiphilic hyperbranched multi-arm copolymer was added to a selective solvent, macroscopic tubes with centimeter-scale length and millimeter-scale diameter appeared. The hyperbranched multi-arm copolymer (HBPO-star-PEO; Fig. 1) is an amphiphilic macromolecule with a hydrophobic hyperbranched poly(3-ethyl-3-oxetanemethanol) core (HBPO) and many hydrophilic poly-

(ethylene glycol) arms (PEO). The molecular weight of the core precursor, as characterized by size exclusion chromatography (SEC), is 8560 (10,500 by the vapor-pressure osmometer); the polydispersity index is 1.5, and the degree of branching measured by ^{13}C nuclear magnetic resonance (NMR) is 0.45 (14). When 3 g of the dried viscous jelly-like HBPO-star-PEO was directly added to 30 ml of acetone under stirring conditions at room temperature, macroscopic tube self-assembly was observed. [Details of the preparation, characterization, and self-assembly of HBPO-star-PEO are given in (14).] A photograph of the resulting self-assembly objects (Fig. 2) reveals transparent tubes that can be seen with the naked eye. The diameter of the tubes approaches 1 mm, and the average length of the tubes is about 1.8 cm (except those broken by vigorous stirring). The length of the longest tubes formed in other batches approaches 7.5 cm, and the diameter of the largest tube is 1.5 mm (15). In addition, there are a number of imperfect tubes in Fig. 2. For instance, object **a** is a fractured tube that mediates between a tube and a film, and object **b** is a twin tube made of a curly film.

The macroscopic morphology of the tubes was also observed by optical microscopy. A pentawalled tube with the coaxial cylindrical

College of Chemistry and Chemical Engineering, Shanghai Jiao Tong University, 800 Dongchuan Road, Shanghai, 200240, People's Republic of China.

*To whom correspondence should be addressed. E-mail: dyyan@sjtu.edu.cn

REPORTS

structure (Fig. 3A) has an outer diameter of 1 mm, and the thickness of a single wall is around 400 nm (Fig. 3B). Most of the tubes have a similar inner diameter, uniform wall thickness, and almost equal distance between two neighboring walls; the outer diameter of a tube mainly depends on the number of its walls. Two terminal types of the tubes (Fig. 3, C and D) suggest that a multiwalled tube consists of only one membrane and grows with the formation of the screw structure.

The tubes are stable in organic solvents. Before the self-assembly, the synthesized HBPO-star-PEO dissolves in polar solvents such as *N,N*-dimethylformamide (DMF) and dimethyl sulfoxide (DMSO), but after molecular assembly the tubes are insoluble in DMSO, DMF, and other polar solvents except trifluoroacetic acid (TFA). In TFA the self-assembly tubes gradually disappeared after 1 week at room temperature (25° to 35°C). Some of the hydroxyl groups in the tubes had reacted with TFA to form the ester groups during the “dissolution” process, and after removing the TFA the residual material could no longer self-assemble in acetone (14). No change was observed for the tubes after immersion in acetone for at least half a year.

These tubes are flexible, and they can be bent in solvent to form a crossed knot pattern without any fracture. In addition, when a tube is taken out of acetone and dried on glass, it collapses into a ribbon-like object. However, it can recover its tubular shape if the ribbon-like object is immersed in acetone once more.

The copolymer composition is important for the macroscopic molecular self-assembly. The tube yield was relatively low. Only about 10% of the synthesized multi-arm copolymer underwent the molecular self-assembly, and the remainder dissolved in acetone. Quantitative magic angle spinning (MAS) solid-state ¹³C NMR was used to characterize the self-assembled part of the synthesized HBPO-star-PEO copolymer (14). The spectrum

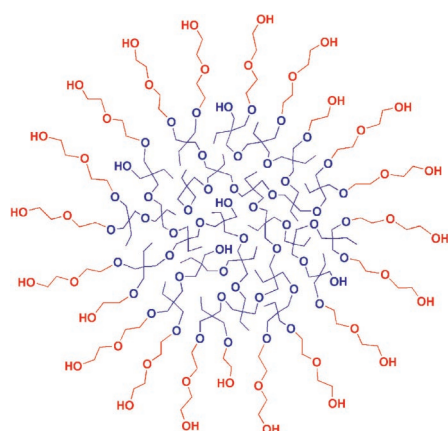


Fig. 1. Diagrammatic sketch of the HBPO-star-PEO multi-arm copolymer. Green, HBPO core; red, PEO arms.

shows that the molar ratio of ethylene oxide units to 3-ethyl-3-oxetanemethanol units (the mole hydrophilic ratio) is 5.14, and that ~28% of the hydroxyl groups of the hyperbranched cores remain unreacted, so the number-average degree of polymerization of PEO arms is about 7. We take account of the 90% residual multi-arm copolymer that does not take part in the self-assembly. The characterization with quantitative MAS solid-state ¹³C NMR shows that the PEO arms of the 90% residual multi-arm copolymer are longer than those of the self-assembled part (Table 1). The detailed characterization of HBPO-star-PEO molecules by SEC (Table 1) shows that the copolymer that forms tubes has a lower molecular weight and a narrower molecular weight distribution than the residual copolymer that does not participate in the self-assembly. The copolymer before the self-assembly has a molecular weight between those of the self-assembled part and the residual non-self-assembled part of the copolymer, and has an even broader molecular

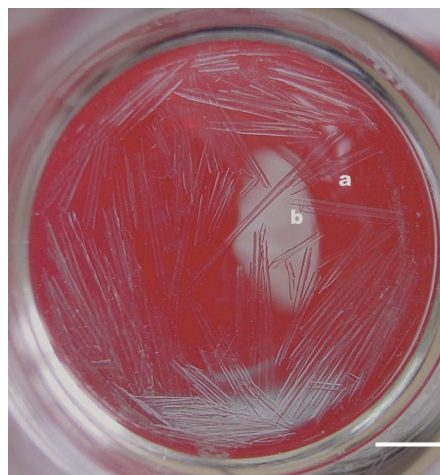


Fig. 2. Macroscopic molecular self-assembly tubes from the HBPO-star-PEO multi-arm copolymer. The photo was recorded from the bottom of a glass beaker, with red paper as the background. An open tube (a) and a twin tube (b) are shown. Scale bar, 1 cm.

weight distribution. Evidently, only a part of the HBPO-star-PEO molecules with suitable length of the PEO arms and hydrophilic ratio can self-assemble into the macroscopic tubes, and the major part of the copolymers with longer PEO arms does not separate from acetone, so it fails to self-assemble.

Besides the molecular structure, the macroscopic self-assembly of HBPO-star-PEO copolymer is also affected by other factors such as the nature of the selective solvent, the copolymer concentration, the added ions, and the self-assembly procedure. For instance, the self-assembly had been conducted in water, ester, alcohol, and other solvents, but the macroscopic tubes were observed only in acetone and were obtained only when the copolymer concentration in acetone ranged from 10 mg/ml to 1 g/ml. The self-assembly morphology was influenced as well by the pH and ionic strength of the medium, and macroscopic membranes were found in a suitable pH or ionic strength in acetone. In addition, the preparation procedure is important for the self-assembly process. When the copolymer-DMF solution was put into acetone, as was done for the preparation of crew-cut micelles

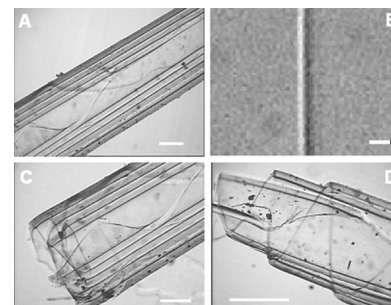


Fig. 3. Optical microspectroscopy images of the tubes in acetone. (A) A pentawalled self-assembly tube. One of the dark lines shows a single wall, and the space between two lines is vacant. (B) Image of a single wall. (C) An internal screw end of the self-assembly tube. It is a left-hand screw. (D) An external screw end of the self-assembly tube. It is a right-hand screw. Scale bars, 300 μm [(A), (C), (D)], 1 μm (B).

Table 1. Characterization of core precursor and HBPO-star-PEO samples. M_n , number-average molecular weight.

Samples	M_n (g/mol)	Polydispersity index	Mole hydrophilic ratio
HBPO core precursor	8,560	1.5	—
Copolymer before self-assembly	36,660	2.7	8.20
Copolymer constituting tubes			5.14
After end-capping	32,789	1.46	
Subtracting end groups	40,340*	1.6*	
Residual copolymer not participating in self-assembly	25,020	—	
	31,570*	—	
	42,202	2.0	9.46

*The characterization was conducted using SEC with a multi-angle light-scattering detector and THF as the solvent. Other molecular weight data were measured by SEC with a refractive index detector and DMF as the solvent.

(1, 2), saddle-like macroscopic membranes instead of tubes appeared (fig. S5).

^1H NMR studies show that the surface of a tube is covered by highly ordered and tightly packed PEO arms (14). Given that the thickness of the tube wall is about 400 nm and the size of a single HBPO-star-PEO macromolecule is about tens of nanometers (as inferred from its molecular weight), how do the HBPO-star-PEO macromolecules aggregate into such a multiwalled tube? To address this question, we used transmission electron

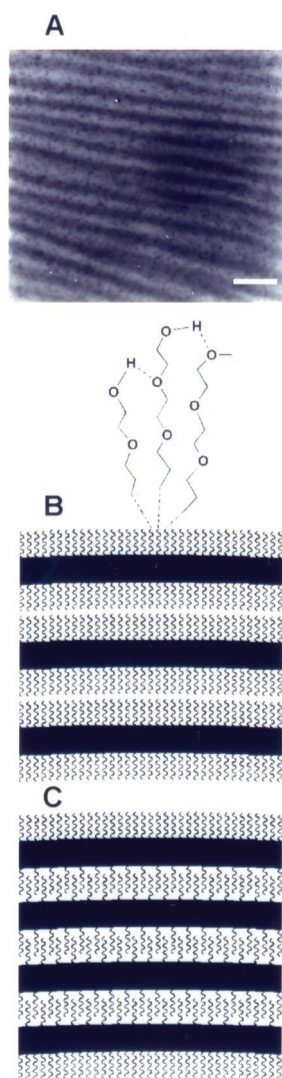


Fig. 4. (A) TEM micrograph of the cross section of the macroscopic molecular self-assembly tube wall. Scale bar, 25 nm. (B and C) Stacking pattern of the macroscopic self-assembly tube wall. The tube wall was formed by the stacking of the sandwich-like nanomicrofilms. (B) Juxtaposed model. (C) Interdigitated model. The green zones represent the condensed HBPO cores; the red wave curves denote PEO arms; the exaggerated part on the top of (B) shows three arms and the hydrogen bonds among them; and hydrogen bonds within core zones and between sandwich layers are omitted. The illustrations are not drawn to scale.

microscopy (TEM) to investigate the morphology of the cross section of the tube wall. Uranyl acetate was used as a negative staining agent, which made the PEO phase appear dark. The lamella morphology in Fig. 4A follows the sequence of “black-gray-black,” which corresponds to “PEO-HBPO-PEO,” or alternating lamellae of HBPO cores and PEO arms. The width of the striped domains is not uniform, which can be attributed to the inhomogeneous molecular size and ill-defined structure of the hyperbranched multi-arm copolymer, and differs from the lamella morphology of block copolymers (7, 16).

The lamella morphology of tube wall indicates that microphase separation plays an important role in the molecular self-assembly of the hyperbranched multi-arm copolymer. In the selective solvent acetone, the hydrophobic interaction of the HBPO cores of the amphiphilic hyperbranched multi-arm copolymer leads to a spinodal microphase separation. The HBPO cores aggregate together in acetone during the microphase separation, and this process is accompanied by the spontaneous segregation of HBPO cores and PEO arms. The phase of the aggregated cores should have a sufficiently large surface for the residence of the large population of arms. The aggregated PEO arms extend out from the interfaces between cores and arms because of the hydrophilic nature of PEO and the repulsion among arms. With the segregation of HBPO cores and PEO arms, the distance between hydroxyl and ether groups or among hydroxyl groups in both arms and cores decreases and facilitates the formation of hydrogen bonds. Hydrogen bonds in both core and arm lamellae can further drive the molecular self-assembly process and strengthen the macroscopic self-assembly tubes. The dissolution of the self-assembled tubes in organic solvents after destruction of the hydrogen bonds verifies the important effect of hydrogen bonds on the molecular self-assembly [the evidence of strong hydrogen bonds between hydroxyl and ether groups or among hydroxyl groups in the tubes is illustrated in (14)]. Finally, the macroscopic tubes with the lamella wall are formed. We consider that the macroscopic molecular self-assembly of the hyperbranched multi-arm copolymer is induced by microphase separation and further driven by the formation of hydrogen bonds.

We propose two molecular stacking models for the tube walls. In a juxtaposed structure (Fig. 4B), a number of sandwich-like microfilms form, consisting of condensed HBPO cores inside and a large population of oriented PEO arms outside, and these films pile together layer by layer. The PEO arms are highly ordered because of their mutual stereo repulsion. The sandwich microfilms are joined together by the hydrogen bonds between the PEO arms of neighboring micro-

films. In an interdigitated structure (Fig. 4C), the arms from neighboring microfilms interpenetrate. Because a PEO arm of the HBPO-star-PEO copolymer in the macroscopic tubes has 7 ethylene oxide units in average, the theoretical average length of the PEO arms is about 3.5 nm if the arms adopt a completely zigzag stretched conformation (17), and the width of the dark PEO zone in Fig. 4A is about 6 (± 2) nm, so the juxtaposed model seems more preferable and the PEO arms are highly oriented indeed. In these models, the core lamellae are amorphous, and the PEO arms in their lamellae are oriented. Thus, the lamella structure of the tube wall is in the sequence of “ordered-amorphous-ordered,” and the lamella thickness is not uniform. In general, the macroscopic self-assembly tube is made from a single membrane, and the membrane is formed through the layer-by-layer stacking of the alternating lamellae of HBPO cores and PEO arms (14). The lamellae are inhomogeneous and may merge (fig. S7), so the order of macroscopic organization of the tubes is not as perfect as that of a conventional block copolymer.

The formation of hydrogen bonds in both core and arm lamellae strengthens the macroscopic self-assembly tubes and further drives the molecular self-assembly process. The robustness of these tubes should facilitate post-treatments such as surface cross-linking and functional group modification.

References and Notes

1. L. Zhang, A. Eisenberg, *Science* **268**, 1728 (1995).
2. L. Zhang, K. Yu, A. Eisenberg, *Science* **272**, 1777 (1996).
3. F. M. Menger, *Angew. Chem. Int. Ed. Engl.* **34**, 2091 (1995).
4. D. E. Discher, A. Eisenberg, *Science* **297**, 967 (2002).
5. B. M. Discher *et al.*, *Science* **284**, 1143 (1999).
6. R. Oda, I. Huc, M. Schmutz, S. J. Candau, F. C. Mackintosh, *Nature* **399**, 566 (1999).
7. S. I. Stupp *et al.*, *Science* **276**, 384 (1997).
8. J. D. Hartgerink, E. Beniash, S. I. Stupp, *Science* **294**, 1684 (2001).
9. T. Kato, *Science* **295**, 2414 (2002).
10. F. M. Menger, S. S. Lee, X. Tao, *Adv. Mater.* **7**, 669 (1995).
11. G. C. L. Wong *et al.*, *Science* **288**, 2035 (2000).
12. B. N. Thomas, C. R. Safinya, R. J. Plano, N. A. Clark, *Science* **267**, 1635 (1995).
13. J. M. Schnur, *Science* **262**, 1669 (1993).
14. Details of synthesis, self-assembly process, and characterization are available at *Science Online*.
15. D. Yan, Y. Zhou, J. Hou, data not shown.
16. T. Goldacker, V. Abet, R. Stadler, I. Erukhimovich, L. Leibler, *Nature* **398**, 137 (1999).
17. A. Abe, J. E. Mark, *J. Am. Chem. Soc.* **98**, 6468 (1976).
18. We thank A. Müller, Y. Hu, M. Van Beylen, C. Gao, and M. Zhang for discussions and Y. Yao for measuring the MAS solid-state ^{13}C NMR. Supported by the basic research foundation of Shanghai Science and Technique Committee and by National Natural Science Foundation of China grants 50233030, 20274024, and 20304007.

Supporting Online Material

www.sciencemag.org/cgi/content/full/303/5654/65/DC1
Materials and Methods
SOM Text
Figs. S1 to S7

25 August 2003; accepted 20 November 2003